I&EC research
Industrial & Engineering Chemistry Research

Article

Cite This: Ind. Eng. Chem. Res. 2020, 59, 2457−2470

pubs.acs.org/IECR

Process Operability Algorithms: Past, Present, and Future Developments

Vitor Gazzaneo,[†] Juan C. Carrasco,[‡] David R. Vinson,[§] and Fernando V. Lima*[,†]

[†]Department of Chemical and Biomedical Engineering, West Virginia University, Morgantown, West Virginia 26506, United States
[‡]Department of Chemical Engineering, Universidad de Concepción, Concepción, Chile
[§]VinsonTech, LLC, The Woodlands, Texas 77381, United States

ABSTRACT: In this Article, the recently developed multimodel and NLP-based operability approaches are reviewed and further developed in terms of theory, application, and software infrastructure. Classical process operability concepts are also revisited and contrasted with new extensions present in both approaches. A focus is given on the comparison between distinct measures of the operability index and the handling of infeasible portions of the desired operating region. For the software infrastructure outcome, a framework for the development of process operability algorithms is provided. In particular, generated codes from the studied approaches are included in an open-source platform that will grant access of the algorithms to researchers from academia and industry. This platform has the purpose of dissemination and future improvement of process operability algorithms and methods. For the development of a versatile process operability tool, the considered approaches are adapted to support process models of generic dimensionalities. New contributions are also incorporated such as the conventional operability index calculation and other methods to find optimal design regions. Nonlinear energy systems of different input × output dimensionalities (6 × 3, 7 × 3, and 3 × 3) are addressed to demonstrate the applicability of the features available in the developed software tool to process achievability analysis, intensification, and modularization.

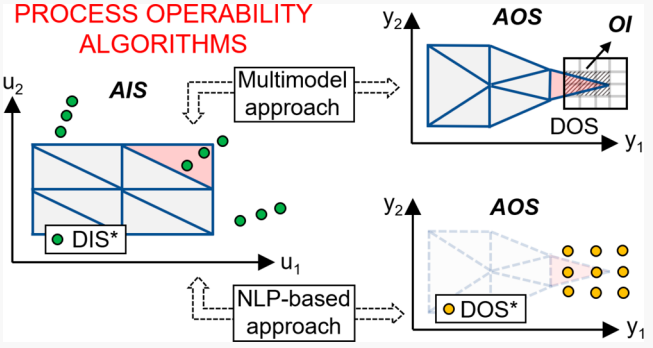

1. INTRODUCTION

Environmental changes have challenged the way natural resources are exploited by industry. Advances in catalysis, materials, and process systems engineering strategies have given rise to novel designs[1,2] allowing more efficient and versatile utilization of feedstocks and resources. Modular and intensified systems are important examples of recent transformations in the conceptualization of process design. These emerging technologies are typically first-of-a-kind designs and present limited heuristics and guidelines associated with process operation. This in turn can result in a design that is susceptible to control infeasibilities.

A viable alternative to the sequential tasks of process design, followed by the selection of control strategies, is the integration of both tasks in early design stages. For this purpose, process operability analysis has emerged as a tool to achieve this integration through quantification of operational uncertainties, disturbances, and constraint violations with the goal of assuring optimality and feasibility.[3] Specifically, the concept of operability index (OI) was introduced as a measure of the capability of a design to consider changes in operational variables, while maintaining controlled variables within a desired achievable range.[3,4] This concept was widely applied to steady-state systems to give insights in the process synthesis phase about future plant operations.[3−6]

Dynamic operability approaches were also developed to extend steady-state operability concepts in order to assess transient output constraints.[7−9] These approaches produced a performance upper bound for achieving operating regions, derived in terms of an idealized controller scenario.

Throughout the development of operability methods, input−output mappings have always been present as an indispensable technique to quantify achievability and controllability.[10] When performing this mapping, intrinsic challenges were brought into the operability analysis such as space nonconvexities, nonlinearities, and system dimensionality. Historically, several approaches were developed to tackle these challenges, mainly either in the field of operability or in the field of flexibility such as (i) surface-response-based techniques (kriging and surface response methods),[11,12] (ii) data-driven experiments and design of experiments,[11−14] (iii) simplicial approximation,[15] (iv) high-dimensional data-driven model representations,[12,16] (v) multiparametric approaches,[17,18] and (vi) metamodeling.[19]

Special Issue: Christos Georgakis Festschrift

Received: September 16, 2019
Revised: December 14, 2019
Accepted: December 23, 2019
Published: December 23, 2019

DOI: 10.1021/acs.iecr.9b05181
Ind. Eng. Chem. Res. 2020, 59, 2457−2470

Recent publications employed another extension of the conventional operability approach considering the design inputs (physical dimensions) instead of the operational inputs of the system.[20−24] These approaches draw special attention when it comes to finding emerging designs that employ the concepts of process intensification (PI) and system modularization (SM). Later approaches considered both design and operational inputs to evaluate and rank competitive designs.[10] These approaches introduced an alternative measure of OI to systematically analyze the achievability of PI targets in a modular design region containing candidate designs for SM and PI. Nevertheless, for the considered approaches, no comparison with traditional measures of OI was established. The employed algorithms were also limited to square systems up to 3 × 3 dimensionality, corresponding to a gap in the operability literature.

Operability algorithms are usually tailored to address specific applications, considering particular dimensionalities and expected system behavior. Thus, a common limitation is the restricted applicability of the produced algorithms. Another challenge comes from the fact that a very limited number of algorithms and codes (if any) have been shared in the reported process operability literature. Consequently, the reproducibility and comprehensive comparison among distinct approaches are hindered, restricting theoretical contributions to isolated applications.

In this Article, current process operability approaches are further developed in terms of theory to tackle a variety of system dimensionalities and applications. The employed optimization formulations are mathematically extended to also handle nonsquare systems. The traditional measure of OI is incorporated, allowing a formal comparison with recently introduced alternative measures. A review of the current approaches and traditional operability concepts and strategies is also provided. Future developments are examined as prospective avenues and challenges to be addressed.

For the software infrastructure contribution, the resulting algorithms are structured and compiled as part of an open-source MATLAB platform named "Process Operability App Project" that will grant access to available operability algorithms for the research community. The theoretical developments and software tool are illustrated via applications that include the direct methane aromatization membrane reactor (DMA-MR) and cycling of the carbon capture and storage (CCS) subsystem of a coal-fired power plant. Specific information about the development of the algorithms for incorporation into the operability tool is also presented throughout the Article.

This Article is structured as follows: section 2 contains previous process operability developments; section 3 reviews basic operability concepts; in section 4, current process operability algorithms and new contributions are described; section 5 shows the applications; and, in section 6, conclusions and future developments are discussed.

2. PROCESS OPERABILITY: SUMMARY OF PRIOR WORK

Process operability was originated for the assessment of linear and nonlinear steady-state systems.[3] The first studies described fundamental system characteristics, achievability of desired operating regions, and which possible changes in the design could be considered for improvement of process operation. The incorporation of process dynamics into operability consisted of a complemental analysis that provided detailed information about transient operation and applicability to specific control strategies. It is important to note that, except for intrinsically dynamic systems, the steady-state analysis is suggested as either a primary or sole analysis, which can possibly be supplemented by dynamic operability.[9] A summary of prior work is given in the following subsections.

2.1. Steady-State Analysis. The calculation of regions for set point and disturbance rejection control motivated the creation of the OI. Input−output mappings were employed to describe inherent process behavior and facilitated the analysis of nonlinear systems, which were not suitable to conventional linear controllability measures. A systematic generalized approach for both linear and nonlinear square systems enabled the determination of necessary inputs to compensate for the presence of disturbances and/or to achieve desired set points. The OI, in turn, quantified the capability of the system to comply with both tasks of set point control and disturbance rejection.

The expansion to nonsquare systems was accomplished by adopting concepts of optimization and interval control.[25] With fewer degrees of freedom, some of the controlled variables could not be set point controlled but were able to be controlled within a determined output interval. Conversely, with extra degrees of freedom, optimization-based frameworks had to be employed along with either economic or performance objectives to accommodate the presence of additional input variables.[6,26]

Operability analysis was then extended to consider design variables. The method for verification of regions for set point control and disturbance rejection was employed to find the portion of the design space that minimized the process footprint, cost, and achieved PI targets while respecting process constraints.[20−23] A nonlinear-programming (NLP)-based formulation was considered to perform direct and inverse input−output mapping calculations.

To obtain faster computational times, a multimodel variation of this formulation adopted multiple linearized models to represent the input−output mapping as a set of connected input−output polytopes.[24] The optimization formulation was then cast as a mixed-integer linear programming (MILP)-based problem. Nevertheless, both NLP-based and multimodel approaches had as the main outcome an input point associated with the most intensified modular design and no calculation of the OI was initially performed.

A recent approach introduced a multilayer operability framework to combine the tasks of finding intensified modular designs and quantifying the system's ability to achieve set point control regions.[10] This approach extended the multimodel framework with MILP-based formulation not only to consider an intensified modular point but also to evaluate candidate designs in a modular design region using the OI, thus taking into account process operation. Particularly, a new method for the OI calculation was introduced as an alternative for the conventional measures of length, volume, and hypervolume. This new method quantified the achievability of output subregions and allowed the calculation of the OI for output regions that are described by shapes with small hypervolumes.

Although the use of the OI consisted of an effort reported for the first time in the PI and SM operability literature, process operability was left with two possible measures of OI, the classical measure with hypervolumes and the newly introduced measure in terms of subregions. As no guidance was provided regarding the selection of OI measure, the formal comparison between these two measures is still a gap. A common challenge associated with operability approaches is the generation of algorithms that tackle either square or nonsquare systems of

DOI: 10.1021/acs.iecr.9b05181
Ind. Eng. Chem. Res. 2020, 59, 2457−2470

specific dimensionalities and thereby present restricted reproducibility.

This Article explores the further development of the NLP-based and the multilayer operability approaches. For comparison between OI measures, the multilayer approach is augmented by incorporating the conventional measure of OI. To overcome the challenges of system dimensionality and reproducibility, the NLP-based and multilayer approaches are generalized to handle square and nonsquare systems with extra degrees of freedom. The developed codes are included as part of the Process Operability App Project, enabling the employment of user-entered functions associated with the desired applications.

2.2. Dynamic Analysis. The study of the minimum time required for a considered process to perform the tasks of set point control and disturbance rejection incited the development of dynamic operability.[7,27] A dynamic form of the OI was formulated, accounting for the desired dynamic performance and intrinsic dynamic system behavior. In particular, the dynamic OI provided insights about the system compatibility with dynamically controlled operation, indicating whether controllability should be further investigated or immediately rejected due to the system's inability to respond within a desired operating time.

Later, other dynamic operability approaches addressed problems with fewer degrees of freedom by adopting the ideas of interval-controlled output variables.[8] Particularly, the output variables were analyzed during transient operation and the outcome resulted in an output region represented by a funnel with dynamic outputs constraints. In this Article, focus will be given to steady-state operability analysis. A historical description of dynamic operability can be found in ref 6.

3. PROCESS OPERABILITY: THE BASIC CONCEPT

The system dimensionality and objectives in the operability analysis determine how major concepts can be adapted and applied to each case. For example, when evaluating disturbance rejection, the OI may be calculated from an input or output perspective. In this section, generic operability concepts are explained along with the particularities for steady-state scenarios.

Set point operability is focused on the study of square systems. Considering a system with m inputs, n states, p outputs, and q disturbances, the following process model, M, may describe the system behavior:

$$M = \begin{cases} \dot{x} = f(x, u, d) \\ y = g(x, u, d) \\ h_1(\dot{x}, x, y, \dot{u}, u, d) = 0 \\ h_2(\dot{x}, x, y, \dot{u}, u, d) \geq 0 \end{cases} \quad (1)$$

in which $x \in \mathbb{R}^n$ are the state variables, $y \in \mathbb{R}^p$ are the outputs, $u \in \mathbb{R}^m$ are the inputs and $d \in \mathbb{R}^q$ are the disturbances. f: $\mathbb{R}^{m+n+q} \rightarrow \mathbb{R}^n$ and g: $\mathbb{R}^{m+n+q} \rightarrow \mathbb{R}^p$ are nonlinear maps. h_1 and h_2 are equality and inequality process constraints, respectively. Furthermore, $\dot{x}$ and $\dot{u}$ represent time derivatives associated with x and u, respectively.

With the above notation, three basic operability sets can be readily defined, as follows.

Available Input Set (AIS). This set of available inputs may be changed within a certain range according to accessibility. It may represent operational inputs and/or design inputs. Operational inputs are manipulated variables (MVs), the subject of control studies, whereas design inputs are associated with available designs (available material, dimensions, etc.). Mathematically, the AIS is given by

$$\text{AIS} = \{u \in \mathbb{R}^m | u^{\min} \leq u \leq u^{\max}\} \quad (2)$$

When needed, the AIS can be distinguished by sets that solely comprise design variables ($\text{AIS}_{\text{des}} \in \mathbb{R}^{m_{\text{des}}}$) or operational variables ($\text{AIS}_{\text{op}} \in \mathbb{R}^{m_{\text{op}}}$), in which m_{des} and m_{op} are the dimensionalities of AIS_{des} and AIS_{op}, respectively. In case both types of input variables are present, the complete AIS is a result of the Cartesian product $\text{AIS}_{\text{des}} \times \text{AIS}_{\text{op}}$ with $m = m_{\text{des}} + m_{\text{op}}$.

Desired Output Set (DOS). This set represents the desired region of operation. It may be defined, for example, by process constraints and desired production or efficiency. Mathematically, the DOS is given by

$$\text{DOS} = \{y \in \mathbb{R}^p | y^{\min} \leq y \leq y^{\max}\} \quad (3)$$

Insights about the determination of the DOS may be given by input−output mappings using the AIS and the Achievable Output Set (AOS) defined below. For example, given an AIS that represents available process conditions for MVs, an AOS with achievable controlled variables can be generated through direct mapping. By inspecting the generated AOS, achievable zones may be analyzed for selecting the best operating output region according to economic or environmental targets. Experimental recommendations are also important factors in the selection of the DOS; i.e., system pressure and temperature limits should not be exceeded in order to preserve mechanical and chemical integrity of structures (e.g., structure of metals for catalysts, membranes, and so on).

Expected Disturbance Set (EDS). This set of expected disturbances, also representing process uncertainties, is mathematically defined as

$$\text{EDS} = \{d \in \mathbb{R}^q | d^{\min} \leq d \leq d^{\max}\} \quad (4)$$

For a system without perturbations (i.e., disturbances are kept in their nominal values), the EDS is defined by

$$\text{EDS} = d^N \quad (5)$$

where $d^N \in \mathbb{R}^q$ is a vector composed of fixed nominal values.

Considering the process model M, the inverse model M^{-1}, and the sets above, other operability sets can be calculated as described below.

Achievable Output Set (AOS). This is a set of controlled variables that the system can achieve for the considered AIS and EDS. This set is generically defined as a function of inputs and disturbances. For each disturbance scenario, $d \in \text{EDS}$, the AOS can be obtained as follows:

$$\text{AOS}_u(d) = \{y \in \mathbb{R}^p | y = M(u, d) \text{ and } u \in \text{AIS}\} \quad (6)$$

If disturbances are kept in their nominal values, the AOS is a region described by

$$\text{AOS}_u(d^N) = \{y \in \mathbb{R}^p | y = M(u, d^N) \text{ and } u \in \text{AIS}\} \quad (7)$$

When disturbance changes are present, the definition of the AOS will depend on the regulatory action consideration. If no disturbance rejection is considered, the AOS is the conservative region where one can guarantee achievability despite the presence of disturbances, which is described as

DOI: 10.1021/acs.iecr.9b05181
Ind. Eng. Chem. Res. 2020, 59, 2457−2470

$$\mathrm{AOS} = \cap_{d\in \mathrm{EDS}}\, \mathrm{AOS}_u(d) \tag{8}$$

Conversely, to verify achievability for cases in which regulatory action is considered, the operability analysis can be performed from the input perspective as described below by studying the required input changes to compensate for the presence of disturbances.

Desired Input Set (DIS). This is a set of required inputs needed to achieve the entire DOS. It can be computed by applying the inverse model to all the elements in the DOS. For each $d \in$ EDS, this set is generically described by

$$\mathrm{DIS}_y(d) = \{u \in \mathbb{R}^m | M^{-1}(y, d) \text{ and } y \in \mathrm{DOS}\} \tag{9}$$

Without disturbance changes, the DIS is an inverse mapping of the AOS, calculated by using a fixed $d^N \in \mathbb{R}^q$ for the achievement of the entire DOS, described as follows:

$$\mathrm{DIS}_y(d^N) = \{u \in \mathbb{R}^m | M^{-1}(y, d^N) \text{ and } y \in \mathrm{DOS}\} \tag{10}$$

When disturbance changes are considered, the DIS is calculated by using the EDS and DOS, being enlarged to account for the necessary input changes to compensate for the presence of disturbances and achieve the DOS. In that case, the DIS can be calculated to achieve the complete DOS region as

$$\mathrm{DIS} = \cup_{d\in \mathrm{EDS}}\, \mathrm{DIS}_y(d) \tag{11}$$

Cases in which disturbances exist, but no regulatory action is taken are usually addressed from the output perspective, by restricting the AOS, as described above.

Calculations of the DIS can be prone to challenges, either because of the complexity of the process model inversion or the infeasibility of desired targets. Complex process models are frequently present in nonlinear systems that require a nonlinear model, M. Thus, for those cases, the derivation of M^{-1} may not be straightforward. Other challenges are the presence of input−output multiplicities, i.e., two or more input points generate the same output, singularities, nonconvexities, and topological discontinuities. The input and output spaces can be carefully inspected in advance in order to avoid working on problematic regions. Such inspection can be performed by using the Operability App functionalities of input−output mapping and the NLP-based approach for model inversion.

A possible source of infeasible desired operation comes from the arbitrary selection of the DOS. The DOS is commonly selected according to desired measures of production and efficiency that may not be completely achievable. In this case, portions of the DIS calculation are unachievable, since no input points can be mapped to the infeasible outputs. In this Article, linear and nonlinear optimization tools are explored in section 4 to enable the numerical computation of M^{-1} and the handling of possible infeasible points.

With the calculated sets above, determinations of OI can take place. Without regulatory action, the AOS is utilized as the basis to quantify the system's achievability of a desired operating region. With the obtained AOS (eq 8), the OI is associated with servo operation and, when distinction is needed, it is denoted as servo-OI. The servo-OI is described as

$$\mathrm{OI} = \frac{\mu(\mathrm{AOS} \cap \mathrm{DOS})}{\mu(\mathrm{DOS})} \tag{12}$$

in which μ indicates the quantification of regions. For 1-dimensional cases, it can be a measure of length; for 2-dimensional cases, area; for 3-dimensional-cases, volume; and for n-dimensional cases, hypervolume. Alternative quantifications of these regions have also been reported in the recent literature considering the achievement of DOS subregions.[10] A comparison between the volumetric measure and the measure with subregions is provided in section 5.

Without disturbances and perturbations, the servo-OI can also be calculated from the inputs perspective by substituting the DOS and the AOS in eq 12 with DIS and AIS, respectively, i.e., $\mu(\mathrm{AIS} \cap \mathrm{DIS})/\mu(\mathrm{DIS})$. Similarly, when disturbances are present, the quantification of the OI is also performed from the inputs perspective but called regulatory or overall-OI, as it indicates the system's ability to reject disturbances and simultaneously achieve the DOS.

For nonsquare systems with more outputs than inputs, the aforementioned concepts can be adapted for interval operability. The study of output constraints is of particular importance for approaches that address this variation of process operability. More information about interval operability can be found in ref 28.

4. OPERABILITY ALGORITHMS

In the past few years, classical operability algorithms have been extended for the design of emerging energy systems.[10,20,22] These systems are usually not only characterized by a strong nonlinear behavior but also by highly constrained environments. As an example, novel intensified technologies have been developed for modular natural gas utilization, and current operability algorithms can play an important role by ensuring optimal and feasible operation of such technologies.[10,23]

The optimization-based algorithms (NLP and MILP) formulated in recent operability approaches are discussed here. These algorithms are further developed, being generalized in terms of dimensionality and applicability to nonsquare cases. As software contribution, all of the developed codes are compiled as part of the open-source process operability platform, which is used for the applications in section 5. Then, a perspective from how traditional operability challenges are tackled is given along with a description of the algorithms.

4.1. NLP-Based Approach. The NLP-based operability approach has a solid foundation on the calculations of the DIS. As an alternative to the analytical calculation of M^{-1}, an NLP-based optimization problem is formulated, aiming to obtain the elements in the AIS that can achieve a determined DOS. Originally created for square systems, this algorithm can also be applied to nonsquare systems with extra degrees of freedom. Previous applications contained optimization levels that were focused on obtaining an intensified input point associated with modular dimensions and an optimal nominal operation. Nevertheless, the robust calculations of M^{-1}(DOS) are versatile and suitable for other operability purposes.

The concepts of feasible DIS (DIS*) and feasible DOS (DOS*) are introduced to tackle situations in which not all the desired output points are achievable. The DIS* elements are mapped to DOS* elements, and these sets are the outcome of the optimization formulation. The DOS* is the closest set in terms of distance to the initially defined DOS; and the DIS* is the set with the correspondent input elements, obtained through mapping of the DIS*, as DIS* = M^{-1}(DOS*).

The employed optimization formulation initially considers a DOS given by output ranges. This DOS is discretized, generating a set of desired output elements. Then, an error minimization problem is posed, in which, the objective function is to minimize the distance between the feasible and the desired

DOI: 10.1021/acs.iecr.9b05181
Ind. Eng. Chem. Res. 2020, 59, 2457−2470

output elements. With the notation for $m \times n \times p$ systems adopted in section 3, this minimization problem is described below for each jth element of the discretized DOS, $y_j \in$ DOS.

$$\text{P1:} \quad \phi_j = \min_{u_j^*} \rho(y_j, y_j^*) \tag{13}$$

subject to

$$\text{nonlinear model (eq 1)}$$

$$u^{\min} \le u_j^* \le u^{\max}$$

$$c_1(u_j^*) \le 0$$

$$c_2(u_j^*) = 0$$

in which y_j is an element of the discretized DOS, y_j^* is an element of DOS*, u_j^* is an element of DIS*, $M(u_j^*) = y_j^*$, where M is the nonlinear process model defined above, ρ is the relative distance function between $y_j \in$ DOS and $y_j^* \in$ DOS*, $u^{\min}$ and $u^{\max}$ are the lower and upper inputs bounds, respectively, c_1 is an optional set of linear and nonlinear inequality constraints, and c_2 is an optional set of linear and nonlinear equality constraints. Note that the lower and upper input bounds can be set outside of the AIS limits to obtain feasible elements outside of the original available limits. Here, the following form of distance function ρ is considered:

$$\rho(y_j, y_j^*) = \sum_{i=1}^{p} ((y_{i,j} - y_{i,j}^*)/y_{i,j})^2 \tag{14}$$

in which the subscript i indicates the coordinates of $y_j = (y_{i,j})_{i\in\{1,2,\ldots,p\}}$ and $y_j^* = (y_{i,j}^*)_{i\in\{1,2,\ldots,p\}} \in$ DOS*. Note that other metrics could be applied to define this distance, such as absolute value and other norms.

After the feasible sets are obtained, another optimization level can be applied. Employing DIS* and DOS*, the following problem is formulated to attain a determined target (for instance, performance, cost, PI targets, environmental targets, and so on):

$$\text{P2:} \quad \Omega = \max_{u^*} \varphi(u^*, y^*) \tag{15}$$

subject to

$$u^* \in \text{DIS*}$$

$$y^* \in \text{DOS*}$$

in which u^* and y^* are elements of the DIS* and DOS*, respectively, and $\varphi(u^*, y^*)$ is a generic objective function that can represent any of the aforementioned targets. For many cases, this optimization level is translated to a selection of elements from P1, allowing an easy inclusion of bound constraints and linear or nonlinear constraints.

Updated developments for this approach consisted of simultaneously solving the problems P1 and P2 by elaborating a bilevel optimization formulation that combines the inverse model calculation and the attainment of desired targets in tandem. Computer parallelization has also been added to the bilevel formulation as a way to increase the speed of nonlinear calculations. For details on these developments see ref 20.

Both P1 and P2 are generalized here in the introduced Operability App to receive any process model and system dimensionality. The codes are written in MATLAB with the embedded nonlinear solver "fminsearch". Validations of this tool are done by using square and nonsquare systems with extra degrees of freedom. In particular, in section 5, an example using a nonsquare system of dimensionality 7×3 can be found.

4.2. Multimodel Approach. The multimodel approach applies space discretization techniques to represent the input−output mapping as multiple linearized models. These models are structured as connected input−output polytopes, facilitating the computation of space intersections and hypervolumes. The inverse model and other calculations are performed in terms of polytopes and barycentric interpolations, resulting in a reduced computational time in comparison to the NLP-based operability approaches.[10,24]

Generally, the multimodel approach is applied to obtain specific optimized points or regions containing design candidates. Calculations of OI are performed and used to systematically rank competing designs. For example, when SM and PI targets are adopted, the outcome is a modular design region containing potential designs that are ranked by using the OI. In this subsection, the multimodel approach is reviewed, and the new contributions are described. Such contributions include the approach generalization in terms of dimensionality, the incorporation of the conventional measure of OI and improvements in the search region for competing designs.

4.2.1. Multimodel Representation. The generation of the first set of polytopes is the initial task to obtain the multimodel representation. Either elements of the AIS or AOS can be used to generate these polytopes. The expected geometrical shapes of these sets indicate that the AIS is better suited for this task. As described in eq 2, the AIS is usually created from ranges, which most of the time allows this set to be evenly decomposed into smaller subsets. Conversely, the AOS has an unpredictable shape and its decomposition into finer subsets may not always be applicable for systematic methods of space discretization.

Then, to obtain the multimodel representation, mesh and triangulation techniques are applied to the AIS elements, generating a set of polytopes. Since each input point has an output counterpart, corresponding output polytopes are therefore also generated. Each kth pair of connected polytopes is represented as follows:

$$P_k^u = \{u_{1,k}, u_{2,k}, \ldots, u_{j,k}, \ldots, u_{J,k}\} \tag{16}$$

$$P_k^y = \{y_{1,k}, y_{2,k}, \ldots, y_{j,k}, \ldots, y_{J,k}\} \tag{17}$$

in which P_k^u and P_k^y are input and output connected polytopes, $u_{j,k} \in \mathbb{R}^m$ and $y_{j,k} \in \mathbb{R}^p$ are the vertices of the input and output polytopes, respectively, J is the total number of vertices, the subscript j is associated with index of elements, and the subscript k is associated with the action of numbering the obtained paired polytopes.

Here, if triangulation techniques are applied after evenly dividing the AIS, the grid elements will be divided into polytopes with $m + 1$ vertices, holding the property of always being convex. If $p = m$, the property of convexity will also hold for the output polytopes, while for $p \neq m$, the same cannot be inferred. Note that overlaps among obtained output polytopes are likely to happen and must be considered for calculations of hypervolume and intersections.

Assuming a total number of K polytopes, the AIS and AOS can be represented as follows.

$$\text{AIS} = \{P_k^u | k \in S\} \tag{18}$$

DOI: 10.1021/acs.iecr.9b05181
Ind. Eng. Chem. Res. 2020, 59, 2457−2470

$$\text{AOS} = \{P_k^y | k \in S\} \tag{19}$$

in which $S = \{1, 2, ..., k, ..., K\}$ is the set with counts for each connected polytope.

4.2.2. MILP-Based Iterative Approach. The MILP-based iterative algorithm is employed to obtain a specific optimized point or a region containing design candidates that achieve chosen targets and objectives. Space resolution is gradually increased while a given objective function is minimized. The objective function can incorporate targets such as SM, PI, product purity, efficiency, environmental aims and so on. Meaningful applications of this method are associated with situations in which the AIS is composed by design inputs and operational inputs are fixed at a certain nominal point.[10]

In each iteration of this algorithm, one MILP-based problem is solved to select the connected pair of polytopes that minimizes the objective function. The achievement of the DOS and the consideration of possible process constraints are incorporated before the solution of the MILP-problem, lowering the number of available polytopes for the optimization problem. As the algorithm moves along, input limits are redefined and smaller polytopes are obtained, promoting a gradual increase in space resolution.

This process can be repeated until the solution stops changing. A measure of relative error and the maximum number of iterations are used for convergence. For this configuration, the outcome of the algorithm is the optimized input−output point.

Alternatively, the region containing designs candidates can be obtained. Two options are considered for this application and improvement of the framework. The first option is to manually set the input region around the optimized input point, which gives more freedom to users who desire to set specific ranges. The second option is to systematically reduce the size of the analyzed AIS to a certain percentage of the original AIS. For the latter, the direction in which the AIS is zoomed in is the one that minimizes the objective function.

The MILP-based formulation is mathematically described below.

$$\chi = \min_{W_k, b_k} \varphi_{\text{linear}}(u, y) \tag{20}$$

subject to

$$0 \le W_k \le 1$$

$$u = \sum (P_k^u \cdot W_k)$$

$$y = \sum (P_k^y \cdot W_k),\ k \in S'$$

$$b_k = \sum W_k,\ b_k \in \{0, 1\}$$

$$\sum b_k = 1$$

$$c_1(u, y) \le 0$$

$$c_2(u, y) = 0$$

$$u^{lb} \le u \le u^{ub}$$

$$y^{lb} \le y \le y^{ub}$$

in which φ_{linear} is a linearized objective function, $W_k = (w_{j,k})_{j\in\{1,2,...,J\}}$ represents the weight of each of vertex j, J is the total number of vertices in each polytope, k, P_k^u, and P_k^y, represent k connected polytopes from the multimodel representation, u and y are the interpolated points associated with the AIS and AOS, respectively, b_k is a binary variable assigned to each pair of polytopes, $S' \subseteq S$ is the index of polytopes that do not have an empty intersection with the DOS and with the feasible region, c_1 and c_2 are optional linear inequalities and equalities, respectively, and u^{lb},u^{ub}, y^{lb}, and y^{ub} are optional bound constraints associated with u and y, respectively. Additional details about iterative algorithm and the multimodel representation are available in ref 10.

Once one design or a design region is considered, calculations of the OI are performed to evaluate and possibly rank competing designs. The AIS with design variables is augmented to account for the effect of manipulated variables, and systematic calculations of the OI as a function of designs are performed. The sequential actions of finding a design region and then ranking its elements using the OI define what is referred in previous work and in this Article as the "multilayer operability framework".[10]

4.2.3. OI Calculation. The multimodel approach originally employs the measure of OI in terms of subregions. First, the DOS is evenly fragmented into a set of subregions. Then, the intersection AOS ∩ DOS is calculated by using computational geometry tools.[29] Each subregion of the DOS is considered to be achieved if there exists at least a point from the calculated intersection that is inside the subregion. The ratio obtained between the number of achieved DOS subregions and the total number of DOS subregions defines this measure of OI. The number of divisions of the DOS is a parameter that can be changed to increase or decrease the number of subregions. For ranking competing designs, it is recommended to have enough divisions so that differences in the calculated values of OI can be detected.

In this Article, the conventional measure of OI is also incorporated into the multimodel approach for comparison purposes. For such a case, the computational geometry tools are employed to obtain the hypervolumes of the sets DOS and AOS ∩ DOS. The volume of AOS ∩ DOS is calculated by using the set complement (DOS\(AOS ∩ DOS) = {$y \in$ DOS|$y \notin$ AOS ∩ DOS}), to overcome the possible presence of overlaps in the output polytopes.

These two measures of OI and the algorithms described above are included in the developed Operability App. In the app, previous algorithms developed for square systems are extended to address nonsquare cases. Also, codes are generalized to accept any number of dimensionalities and the MILP-based formulation is mathematically adapted to accommodate this change. Scripts are created for the tasks of evenly dividing n-dimensional spaces and performing n-dimensional triangulations. For the latter task, previous limitations in calculations for polytopes with up to 3 dimensions are overcome by adopting the MATLAB subroutine "delaunayn" for 4-dimensional and higher triangulations. The developed tool is tested for combinations of square and nonsquare systems with sets up to 5 dimensions.

4.3. Process Operability App. The software infrastructure contribution in this Article is an open-source platform named "Process Operability App Project". The above-described algorithms are structured and compiled in the form of a MATLAB app. A significant effort was dedicated to make the involved scripts as generic as possible, by both addressing a variety of system dimensionalities and writing codes as a function of user-defined process models, sets and configurations.

In addition to the inclusion of the algorithms, a user interface is developed to allow a versatile user-friendly utilization of the developed tools. The NLP-based and the multimodel

DOI: 10.1021/acs.iecr.9b05181
Ind. Eng. Chem. Res. 2020, 59, 2457−2470

approaches are accessible through functionalities such as (i) generate input−output points, (ii) obtain the multimodel representation, (iii) calculate OI, (iv) find a feasible DIS, and (v) obtain an optimal design or a design region. All the computational geometry calculations in the app are performed by using MPT.[29] In terms of dimensionality limitations, preliminary tests indicate that the NLP-based approach is essentially restricted by computational time and the multimodel approach currently handles calculations involving polytopes with up to 5 dimensions. New releases will pursue the increase in system dimensionality and optimization of computational time with the objective of tackling problems of increasing complexity. More information can be found in the app documentation provided in the Web site mentioned below.

This initiative aims not only to aid process systems applications with the use of operability approaches but also to promote dissemination and discussion in academia and industry toward the improvement of the process operability field. The Process Operability App Project can be accessed at https://fernandolima.faculty.wvu.edu/operability-app where the download of the Process Operability App and additional information are available.

5. APPLICATIONS

To demonstrate the capability of the developed tools, applications for both the NLP-based and multimodel approaches are selected. The DMA-MR and the cycling of a CCS subsystem of a coal-fired power plant are complex energy systems considered for this task. Both systems have been the focus of recent studies in the reported literature: the DMA-MR has been employed for modular natural gas utilization;[10,30] and the CCS, as part of an effort to integrate coal-fired power plants to renewable energy.[31]

5.1. DMA-MR Application. By converting methane to the fuel hydrogen and to the value-added chemical benzene, the DMA-MR is a candidate energy system for the modular utilization of natural gas. The modularization of this system potentially benefits the on-site utilization of the shale gas formations in remote locations, eliminating the need for expensive pipelines and elaborate industrial infrastructure usually present in the conventional large-scale processes. Here, PI and SM are enabled by the combination of reaction and separation. This process integration strategy promotes enhanced reactivity by shifting the reaction equilibrium toward the products, which simultaneously induces footprint reduction by combining the two unit operations.

For operability applications, previously developed work addressed the DMA-MR modeling from experimental data, considering the nonoxidative conversion of methane as a two-step reaction mechanism.[32,33] Catalysis and membrane transport studies were employed to obtain adequate reaction kinetics that were suitable to membrane reactors models constituted by a set of ordinary differential equations (ODEs).[30] Figure 1 below shows a schematic cocurrent configuration of the DMA-MR.

The following two-step reaction mechanism is considered for the DMA-MR.

$$2CH_4 \rightleftharpoons C_2H_4 + 2H_2 \qquad r_1 = k_1 C_{CH_4} - k_1' \frac{C_{C_2H_4} C_{H_2}^{\ 2}}{C_{CH_4}} \tag{21}$$

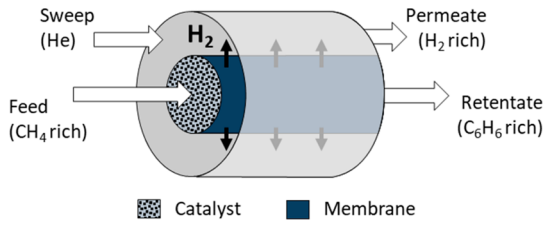

Figure 1. Co-current DMA-MR schematic.

$$3C_2H_4 \rightleftharpoons C_6H_6 + 3H_2 \qquad r_2 = k_2 C_{C_2H_4} - k_2' \frac{C_{C_6H_6} C_{H_2}^{\ 3}}{C_{C_2H_4}^{\ 2}} \tag{22}$$

in which C stands for species concentrations, k_1 and k_2 are the reactions rate constants for first and second steps, respectively, and the prime indicates inverse reaction rate constant.

The generated ODE set from molar balances in the tube and shell can be found in ref 23. Refer to ref 10 for the overall parameters that allow reproducibility of this model (rate constant values, dimensions, nominal values, etc.).

The input and output spaces of this system were already prescreened in previous work.[10,23] This activity consisted of the primary study of the system behavior, which is not addressed in this Article. The outcome is the selection of the sets AIS and AOS and the determination of the DOS. Specifically, in the previous work, the AOS was inspected, and operating output zones corresponding to the highest achievable benzene production and methane conversion were considered. Then, the DOS was determined on the basis of the obtained zones and other experimental indications associated with properties of the membrane and conditions of the reaction.

A total of eight inputs and four outputs is considered for the DMA-MR applications presented in this Article. Tables 1 and 2 show the design and operational input variables and the corresponding available ranges, respectively. Table 3 shows the output variables and the corresponding desired ranges. Each of the studied subsystems have input and output sets of distinct

Table 1. Design Input Variables and Available Ranges

design input variable	available range
reactor length (cm)	10−100
tube diameter (cm)	0.5−2.0
selectivity (−)	300 to 1×10^5
permeance (mol/(s m^2 atm $^{1/4}$))	1×10^{-4} to 1×10^{-2}

Table 2. Operational Input Variables and Available Ranges

operational input variable	available range
methane feed (cm^3/min)	7−9
temperature (°C)	800−1000
sweep gas feed (cm^3/min)	9−11
tube pressure (atm)	1.00−1.12

Table 3. Output Variables and Desired Ranges

output variable	desired range
benzene production (mg/h)	20−25
methane conversion (%)	35−45
hydrogen production (mg/h)	3−6
cost factor (−)	0−100

DOI: 10.1021/acs.iecr.9b05181
Ind. Eng. Chem. Res. 2020, 59, 2457−2470

dimensionalities composed by variables and ranges presented in Tables 1, 2, and 3.

For the modularization of the reactor, the minimization of the process footprint and achievement of PI targets while respecting process constraints are considered. This task is translated to an optimization formulation that is inserted in both NLP- and MILP-based algorithms. The objective function of process footprint, f, is described by the sum of membrane area and reactor volume as follows:

$$f(L, D) = \pi DL + \frac{\pi}{4}D^2L \tag{23}$$

in which L is the reactor length and D is the tube diameter.

One of the employed process constraints is the L/D ratio that assures plug-flow operation,[34] also given as a function of reactor length and tube diameter as follows.

$$\frac{L}{D} \geq 30 \tag{24}$$

Other constraints are included either as bound or inequality constraints as needed, and they are described in each of the applications.

Regarding the utilization of operability algorithms, each of the approaches explored in section 4 is considered for the corresponding DMA-MR subsystem. At first, the multimodel approach is applied to a 6 × 3 subsystem employing the multilayer framework. Then, the NLP-based approach is applied to a 7 × 3 subsystem by using the P1 and P2 formulations. The details of these two applications are discussed below.

5.1.1. DMA-MR Application: 6 × 3 Subsystem. The multilayer framework is employed here to obtain a modular design region and rank designs inside such a region using calculated values of OI. In the first layer of the framework, the MILP-based iterative algorithm is used to find the modular design region, and, in the second layer, calculations of the OI are carried out for the two distinct measures of OI. Then, the obtained results are compared and analyzed for suitability to future applications.

Here, a previously addressed DMA-MR subsystem is considered.[10] The modular design region is constructed from an optimal design point provided by the iterative MILP-based algorithm. Important distinctions from previous work correspond to (i) introduction of the conventional OI measure in terms of hypervolume to the multimodel approach, (ii) comparison between such a measure of OI and the OI in terms of subregions, and (iii) utilization of the Operability App containing a new set of generalized and improved codes.

For the composition of the 6 × 3 subsystem, the AIS $\in \mathbb{R}^6$ comprises three design and three operational inputs. The sets $\text{AIS}_{\text{des}} \in \mathbb{R}^3$ and $\text{AIS}_{\text{op}} \in \mathbb{R}^3$ are employed to distinguish the two types of inputs. The input variables are selected from Tables 1 and 2 and structured as follows:

$$\begin{aligned} u_{\text{des},1} &\overset{\text{def}}{=} \text{Reactor length (cm)} \\ u_{\text{des},2} &\overset{\text{def}}{=} \text{Tube diameter (cm)} \\ u_{\text{des},3} &\overset{\text{def}}{=} \text{Selectivity } (-) \end{aligned} \tag{25}$$

$$\begin{aligned} u_{\text{op},1} &\overset{\text{def}}{=} \text{Methane feed } (\text{cm}^3/\text{min}) \\ u_{\text{op},2} &\overset{\text{def}}{=} \text{Temperature } (^\circ\text{C}) \\ u_{\text{op},3} &\overset{\text{def}}{=} \text{Sweep gas feed } (\text{cm}^3/\text{min}) \end{aligned} \tag{26}$$

in which $u_{\text{des}} = (u_{\text{des},1}, u_{\text{des},2}, u_{\text{des},3})$ and, similarly, $u_{\text{op}} = (u_{\text{op},1}, u_{\text{op},2}, u_{\text{op},3})$. For example, $(15, 0.5, 300) \in \text{AIS}_{\text{des}}$ is a design element associated with reactor length of 15 cm, tube diameter of 0.5 cm, and selectivity of 300.

With the variables and notation above along with the ranges from Tables 1 and 2, the AIS_{des}, AIS_{op}, and the complete AIS are sets, given by

$$\text{AIS}_{\text{des}} = \{u_{\text{des}} \in \mathbb{R}^3 | (10, 0.5, 300) \leq u_{\text{des}} \leq (100, 2.0, 1 \times 10^5)\} \tag{27}$$

$$\text{AIS}_{\text{op}} = \{u_{\text{op}} \in \mathbb{R}^3 | (7, 800, 9) \leq u_{\text{op}} \leq (9, 1000, 11)\} \tag{28}$$

$$\text{AIS} = \{u \in \mathbb{R}^6 | (u_{\text{des}}^{\min}, u_{\text{op}}^{\min}) \leq u \leq (u_{\text{des}}^{\max}, u_{\text{op}}^{\max})\} \tag{29}$$

in which $(u_{\text{des}}^{\min}, u_{\text{op}}^{\min}) = (10, 0.5, 300, 7, 800, 9)$ and $(u_{\text{des}}^{\max}, u_{\text{op}}^{\max}) = 100, 2, 1 \times 10^5, 9, 1000, 11)$.

The AOS contains three outputs, being also a set in $\mathbb{R}^3$. The generation of the AOS can be obtained through direct mapping of the AIS elements using the process model (M). Taking Table 3 as a reference and considering the AIS described by eqs 27−29, the following structure and definition of the AOS are obtained:

$$\begin{aligned} y_1 &\overset{\text{def}}{=} \text{Benzene production (mg/h)} \\ y_2 &\overset{\text{def}}{=} \text{Methane conversion (\%)} \\ y_3 &\overset{\text{def}}{=} \text{Hydrogen production (mg/h)} \end{aligned} \tag{30}$$

$$\text{AOS} = \{y \in \mathbb{R}^3 | y = M(u) \text{ and } u \in \text{AIS}\} \tag{31}$$

in which $y = (y_1, y_2, y_3)$.

The calculation of AOS is not needed for the tasks defined in this application. Since the AOS was already inspected in previous work, a focus is given here on the portions of the AOS that intersect the DOS. Considering the above structure of output variables and the desired ranges in Table 3, the DOS is given by

$$\text{DOS} = \{y \in \mathbb{R}^3 | (20, 35, 3) \leq y \leq (25, 45, 6)\} \tag{32}$$

Given the dimensionality of the above-defined sets, the utilization of the multilayer framework results in the sequential analysis of square systems. In the first layer of the framework, to obtain the modular design region, the operational inputs are fixed at a nominal operation point $u_{\text{op}}^N \in \text{AIS}_{\text{op}}$, defined as $u_{\text{op}}^N = (8, 900, 10)$. The AIS is thus limited in this layer, resulting in the subset $\{(u_{\text{des}}, u_{\text{op}}^N) \in \text{AIS} | u_{\text{des}} \in \text{AIS}_{\text{des}}\}$, simplified to eq 33.

$$\text{AIS}_{\text{layer}_1} = \text{AIS}_{\text{des}} \times u_{\text{op}}^N \tag{33}$$

Note that $\text{AIS}_{\text{layer}_1}$ can be treated as a 3-dimensional set, as only three coordinates associated with AIS_{des} can be changed. As a result, a 3 × 3 square system containing design inputs and outputs associated with a fixed operation is analyzed in the first layer of this framework.

DOI: 10.1021/acs.iecr.9b05181
Ind. Eng. Chem. Res. 2020, 59, 2457−2470

To define the MILP formulation that takes place in the first layer (eq 20), the footprint from eq 23 is linearized[10] and the nonlinear inequality constraint from eq 24 is simply manipulated to assume a linear form. The final form of the objective function including the linearized footprint and inequality constraint are described by eqs 34 and 35, respectively.

$$\varphi_{\text{linear}}(u) = 0.5625u_{\text{des},1} + 12.5u_{\text{des},2} \tag{34}$$

$$-u_{\text{des},1} + 30u_{\text{des},2} \leq 0 \tag{35}$$

For insertion in the Operability App, eqs 34 and 35 are rewritten according to the accepted generalized format. Objective function entries meet the form of $A\begin{bmatrix}u\\y\end{bmatrix}$, while equalities and inequalities meet $A\begin{bmatrix}u\\y\end{bmatrix} \leq b$, in which A and b are used to represent one or multiple linear equations. After this final modification, the obtained equations can be inputted to the Operability App.

The remaining entries for the first layer are the process model, the user-inputted sets, AIS and DOS, and the expected size of the modular design region. The DMA-MR process model is allocated in a MATLAB script and then uploaded to the app. The AIS and DOS are also entered. The option of manually entering a design region around the optimal design is selected for this case.

As a result, the operability app provides the optimal design point $u_{\text{des}}^{\text{opt}} = (17.03, 0.50, 300)$. A design region is created around $u_{\text{des}}^{\text{opt}}$. Values that would be more reasonable for construction/manufacturing can guide the selection of design ranges,[10] generating the following modular design region:

$$\text{MDR} = \{u_{\text{des}} \in \mathbb{R}^3 | (16, 0.50, 500) \leq u_{\text{des}} \leq (18, 0.60, 1500)\} \tag{36}$$

The evaluations of OI are then performed in the second layer of the framework. The activity of fixing $u_{\text{op}}^N \in \text{AIS}_{\text{op}}$ is reversed and for each element $u_{\text{des}}^{\text{MDR}} \in \text{MDR}$, the subset of the AIS $\{(u_{\text{des}}^{\text{MDR}}, u_{\text{op}}) \in \text{AIS} | u_{\text{op}} \in \text{AIS}_{\text{op}}\}$, is simplified to

$$\text{AIS}_{\text{layer}_2} = u_{\text{des}}^{\text{MDR}} \times \text{AIS}_{\text{op}} \tag{37}$$

Note that $\text{AIS}_{\text{layer}_2}$ has properties similar to those of $\text{AIS}_{\text{layer}_1}$, consisting of a set that can be seen as 3-dimensional. A 3 × 3 square system that has operational inputs and outputs and is associated with a design is thus analyzed in this layer of the framework. While $\text{AIS}_{\text{layer}_1}$ consisted of one set associated with the operation u_{op}^N, $\text{AIS}_{\text{layer}_2}$ represents multiple 3 × 3 mappings, each of them associated with one design $u_{\text{des}}^{\text{MDR}} \in \text{MDR}$.

For the calculations of OI, each of these 3 × 3 mappings generates a value of OI. To obtain elements $u_{\text{des}}^{\text{MDR}} \in \text{MDR}$, MDR is discretized. As a result, values $\text{OI} = \text{OI}(u_{\text{des}}^{\text{MDR}})$ are obtained.

For each $u_{\text{des}}^{\text{MDR}} \in \text{MDR}$, the associated $\text{AIS}_{\text{op}} \times \text{AOS}$ mapping undergoes discretization and triangulation, being described by the multimodel representation (in eqs 18 and 19). For the OI in terms of subregions, the DOS is discretized to generate subregions of the DOS. For the volumetric OI calculation, the DOS is kept as it is.

In the Operability App, the uploaded process model and DOS are used. Grids of 11, 3, and 5 elements in each dimension are employed for the discretization of MDR, $\text{AIS}_{\text{layer}_2}$, and DOS, respectively. Justification about the resolution provided by these grids can be found in ref 10.

The app is run twice, first with the measure of OI in terms of subregions and then in terms of volume. For each measure, the complete rank using $\text{OI}(u_{\text{des}}^{\text{MDR}})$ is obtained for each element $u_{\text{des}}^{\text{MDR}} \in \text{MDR}$. Figures 2 and 3 depict the classification of the modular region MDR using OI in terms of subregions and volume, respectively.

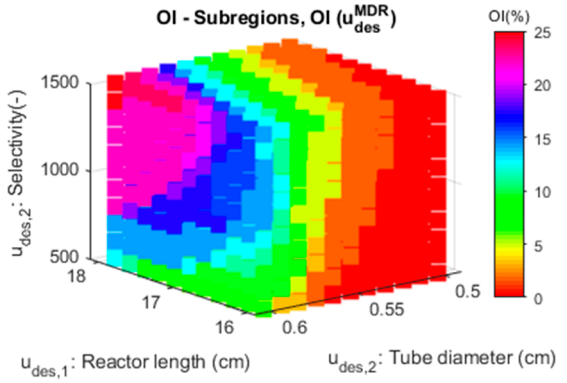

Figure 2. Classification of MDR using OI in terms of subregions.

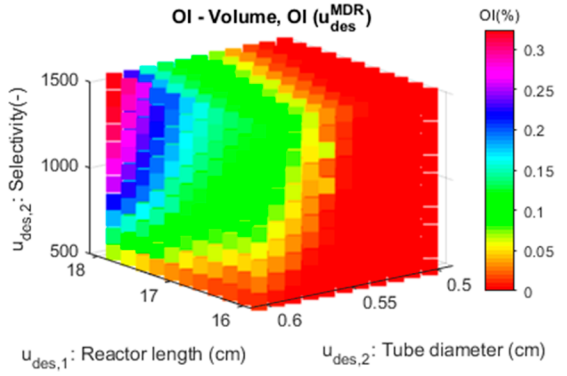

Figure 3. Classification of MDR using OI in terms of volume.

The OI measures using subregions are clearly higher, ranging from 0 to 25%. The measures using volume range from 0 to approximately 0.3%. This difference in magnitude happens because the subregions only require the presence of one point of the AOS to be considered achieved. Therefore, the proportion of achieved subregions tend to be higher than the proportion of achieved volume.

Analyzing the distribution of values of OI inside MDR, Figures 2 and 3 show that both measures present similar trends. Larger membrane reactors provide higher OIs and thus more achievability of the DOS. This classification using OI is in accordance with previous applications of the multimodel framework for this subsystem,[10] showing that the Operability App is able to successfully reproduce existing and improved algorithms.

The differences in the magnitude of OI do not significantly affect the selection of the design with maximum achievability for this application. However, they show that the interpretation of OI in terms of volume may be misleading in some cases. The shape of the AOS is key to understand why this measure can have such low values.

The design of highest OI is selected and the shape of the AOS is analyzed for both calculations of OI. Figures 4 and 5 show the achievement of DOS in terms of subregions and volume, associated with maximum values of OI of 25% and 0.324%,

DOI: 10.1021/acs.iecr.9b05181
Ind. Eng. Chem. Res. 2020, 59, 2457−2470

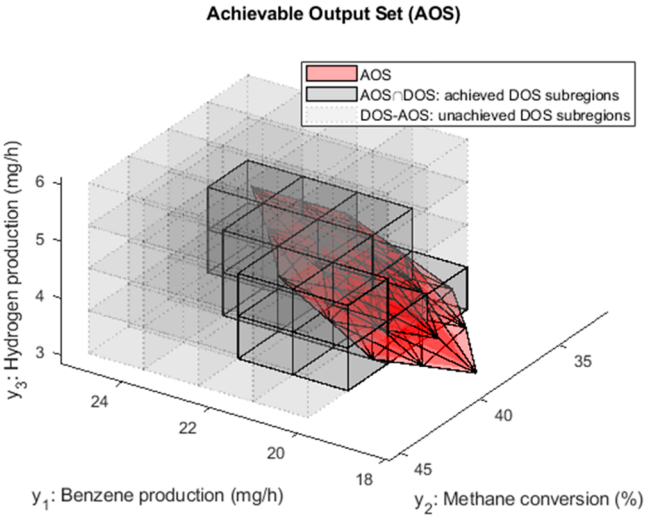

Figure 4. Calculation of output sets in terms of subregions.

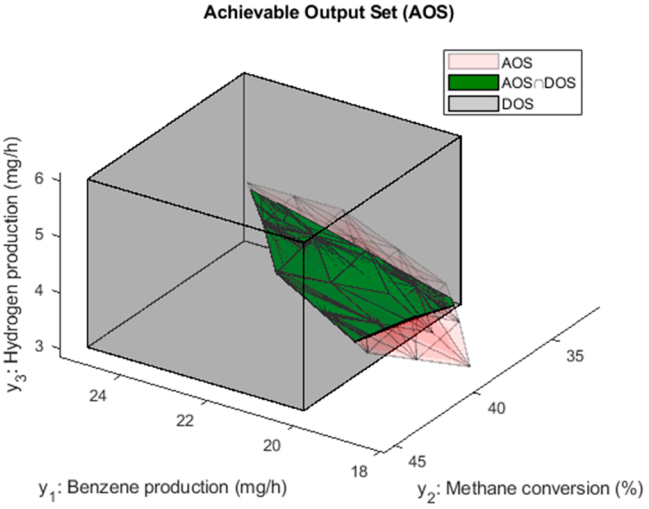

Figure 5. Calculation of output sets in terms of volume.

respectively. The corresponding design is $u_{des} = (18, 0.5, 1500)$ for both cases.

Note from Figures 4 and 5 that the intersections AOS ∩ DOS are given by distinct regions. In Figure 4, the intersection is represented by subregions, whereas in Figure 5, the actual volumes of the intersection and DOS are employed. The visual comparison between the intersections supports the fact that it is easier to achieve portions of subregions of the DOS than portions of DOS in terms of actual volume.

Therefore, the DMA-MR is one example of system in which process integration results in an AOS that almost does not have volume, although it is generated in a 3-dimensional space. For this situation, the volumetric OI may indicate a percentual achievability very small (less than 1%). Nevertheless, as seen from the measure in terms of subregions, the AIS_{op} can be enough to ensure achievability of portions of the DOS, being suitable for future analysis of set point control.

A conclusion is that cases in which the AOS shape is too irregular are susceptible to difficulties in the measure of OI in terms of volume/hypervolume. The measure using subregions provides insights about achievability, being recommended for situations in which the AOS is unknown or presents a strong nonlinear and/or nonconvex behavior. Conversely, if the entire volume of the DOS is desired to be achieved, then the measure of OI that employs hypervolumes is recommended.

5.1.2. DMA-MR Application: 7 × 3 Subsystem. To select the design and the nominal operation that achieve PI targets and minimize process footprint, the NLP-based approach is applied to a 7 × 3 DMA-MR subsystem. The formulation P1 is employed for the determination of the feasible DOS (DOS*), and P2, for the selection of the best input−output point associated with the described goals. This example correspond to a modified case-study presented in ref 35, which addresses the same subsystem but with distinct objectives.

For building the AIS ∈ $\mathbb{R}^7$, four operational inputs and three design inputs are selected. With the same notation as in eqs 25−29 and information from Tables 1 and 2, the AIS is structured as follows:

$$\begin{aligned} u_{des,1} &\overset{def}{=} \text{Reactor length (cm)} \\ u_{des,2} &\overset{def}{=} \text{Tube diameter (cm)} \\ u_{des,3} &\overset{def}{=} \text{Permeance (mol/(s m}^2\text{ atm}^{1/4}\text{))} \\ u_{des,4} &\overset{def}{=} \text{Selectivity (−)} \end{aligned} \tag{38}$$

$$\begin{aligned} u_{op,1} &\overset{def}{=} \text{Methane feed (cm}^3\text{/min)} \\ u_{op,2} &\overset{def}{=} \text{Sweep gas feed (cm}^3\text{/min)} \\ u_{op,3} &\overset{def}{=} \text{Tube pressure (atm)} \end{aligned} \tag{39}$$

$$\begin{aligned} AIS_{des} = \{u_{des} \in \mathbb{R}^4 | &(10, 0.5, 1 \times 10^{-4}, 300) \le u_{des} \\ &\le (100, 2.0, 1 \times 10^{-2}, 1 \times 10^5)\} \end{aligned} \tag{40}$$

$$AIS_{op} = \{u_{op} \in \mathbb{R}^3 | (7, 9, 1.00) \le u_{op} \le (9, 11, 1.12)\} \tag{41}$$

$$AIS = \{u \in \mathbb{R}^7 | (u_{des}^{min}, u_{op}^{min}) \le u \le (u_{des}^{max}, u_{op}^{max})\} \tag{42}$$

in which $(u_{des}^{min}, u_{op}^{min}) = (10, 0.5, 1 \times 10^{-4}, 300, 7, 9, 1.00)$ and $(u_{des}^{max}, u_{op}^{max}) = (100, 2.0, 1 \times 10^{-2}, 1 \times 10^5, 9, 11, 1.12)$.

The set AOS ∈ $\mathbb{R}^3$ has three outputs and, as in the previous application, can be obtained through direct mapping of the AIS elements using the process model, *M*. Here, the complete generation of output points is also not needed, since the input−output space has already been prescreened for the selection of the DOS in previous work. With Table 3 as a reference, the outputs and the DOS are defined as follows:

$$\begin{aligned} y_1 &\overset{def}{=} \text{Benzene production (mg/h)} \\ y_2 &\overset{def}{=} \text{Methane conversion (\%)} \\ y_3 &\overset{def}{=} \text{Cost factor (−)} \end{aligned} \tag{43}$$

$$DOS = \{y \in \mathbb{R}^3 | (20, 35, 0) \le y \le (25, 45, 100)\} \tag{44}$$

In the Operability App, the above AIS and DOS are entered. As in the previous application, the process model is uploaded in the form of a MATLAB script. The nonlinear objective function is inputted as in eq 23, while the process constraint is inputted as in eq 35. To obtain elements in the DOS, a discretization is

DOI: 10.1021/acs.iecr.9b05181
Ind. Eng. Chem. Res. 2020, 59, 2457−2470

employed by informing the Operability App the size of the grid. For being a value that provides a good resolution, a desired grid of 10 elements in each dimension is entered in the app. As additional configuration, the option of generating a solution inside the AIS and DOS is selected.

After running, the Operability App generates the sets DOS* and DIS* as well as the input−output data point that minimizes the process footprint. Figure 6 depicts the DOS* and the

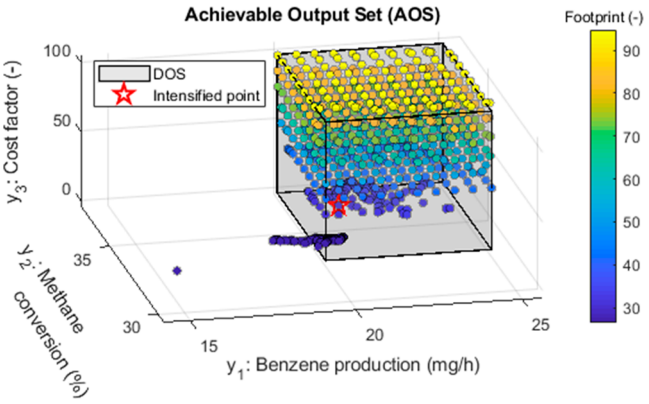

Figure 6. DOS* (color coded points) and intensified point for DMA-MR 7 × 3 application.

selected intensified point, as well the color-coded footprint. The inputs and outputs of the selected intensified design and nominal operation correspond to $u = (16.4, 0.544, 9.97 \times 10^{-3}, 2.44 \times 10^{4}, 7.40, 10.95, 1.002)$ and $y = (20.9, 35.9, 33.7)$ respectively.

An important observation from Figure 6 is that the complete DOS is not achievable. Combinations of high cost factor, benzene production, and methane conversion can be achieved by reactors of large footprints. As the cost factor decreases, the achievability of the DOS is limited. This behavior is expected as the reduction in cost factor is associated with membranes of lower quality, lower catalyst mass, and smaller reactors.[21] The direct relationship between cost factor and footprint derives from the fact that the size of the reactor proportionally affects its associated cost.

As a comparison with previously applied 2 × 2 and 3 × 3 similar subsystems that employed the same objectives, one can notice that the obtained modular design is even smaller. For both previous cases, reported values of reactor length and tube diameter consisted of about 17 and 0.57 cm.[10,23,24] The further reduction in size here is mainly due to the inclusion of operational variables, which present contrasting values with the nominal operation of previously addressed applications, fixed at 8 cm^3/min for methane feed, 10 cm^3/min for sweep gas feed, and 1 atm of tube pressure.

5.2. Cycling of a CCS Unit Application. With the increasing penetration of renewable energy into the power grid, traditional coal-based technologies have to be gradually integrated with wind, solar, and other clean energy sources. The retrofit of existing plants consists of an important example of how these new forms of energy can be coordinated with reliable conventional technologies.

For this application, a CCS unit is analyzed for implementation in a coal-fired power plant. Particularly, to achieve the required power demand, the intermittent behavior of solar and wind energy can be integrated with the generation of energy from coal. A consequent cycling profile is needed from the perspective of the coal-fired power plant, producing variable amounts of flue gas in a day. The CCS unit receives and treats this flue gas, capturing and thereby limiting the emissions of CO_2.

A candidate design of the CCS unit is analyzed here, considering the ranges of MV's and expected amounts of flue gas. The goal of this operability analysis is to determine the maximum CO_2 capture for the employed design and provide insights for possible improvements in operation and design. Here, no quantification of OI is performed, but instead, the input−output mapping with a focus on finding the AOS is explored through the Operability App.

For the CCS system, the selected inputs are exclusively operational, i.e., AIS = AIS_{op}. Besides the flue gas flow rate from the coal-fired power plant, two streams of the CCS are selected. They are associated with the carbon absorption and stripping by the aqueous monoethanolamine (MEA) solvent. The outputs are variables associated with the carbon capture, including the amount of employed solvent and overall work of the CCS unit. Table 4 shows the input variables and selected ranges. Eqs 45 and 46 describe the inputs' structure and the AIS, respectively. Eqs 47 and 48 present the outputs' structure and the corresponding AOS.

Table 4. Input Variables and Available Ranges for CCS Application

input variable	available range
flue gas flow rate (kmol/s)	3.34−3.70
lean MEA solvent flow rate (kmol/s)	9.51−10.75
low pressure steam flow rate (kmol/s)	1.33−1.47

$$u_1 \stackrel{\text{def}}{=} \text{Flue gas flow rate (kmol/s)}$$
$$u_2 \stackrel{\text{def}}{=} \text{Lean MEA solvent flow rate (kmol/s)}$$
$$u_3 \stackrel{\text{def}}{=} \text{Low pressure steam flow rate (kmol/s)} \quad (45)$$

$$\text{AIS} = \{u \in \mathbb{R}^3 | (3.34, 9.51, 1.33) \leq u \leq (3.70, 10.75, 1.47)\} \quad (46)$$

$$y_1 \stackrel{\text{def}}{=} CO_2 \text{capture rate (\%)}$$
$$y_2 \stackrel{\text{def}}{=} \text{Lean solvent } CO_2 \text{loading } (mol_{CO_2}/mol_{MEA})$$
$$y_3 \stackrel{\text{def}}{=} \text{CCS overall work (kW)} \quad (47)$$

$$\text{AOS} = \{y \in \mathbb{R}^3 | y = M(u) \text{ and } u \in \text{AIS}\} \quad (48)$$

in which M refers to the process model, which is the reduced-order model briefly described below.

The three input variables are assumed to be within the ranges that are also adopted to obtain the reduced-order models for the coal-fired power plant. The reduced model for the CCS unit is obtained from previously developed work, by employing system identification techniques. Details about these techniques, the process flowsheet and the cycling operation can be found in ref 36.

For this study, the flue gas flow rate variable is assumed to be a measured disturbance, as it comes from upstream units of the

DOI: 10.1021/acs.iecr.9b05181
Ind. Eng. Chem. Res. 2020, 59, 2457−2470

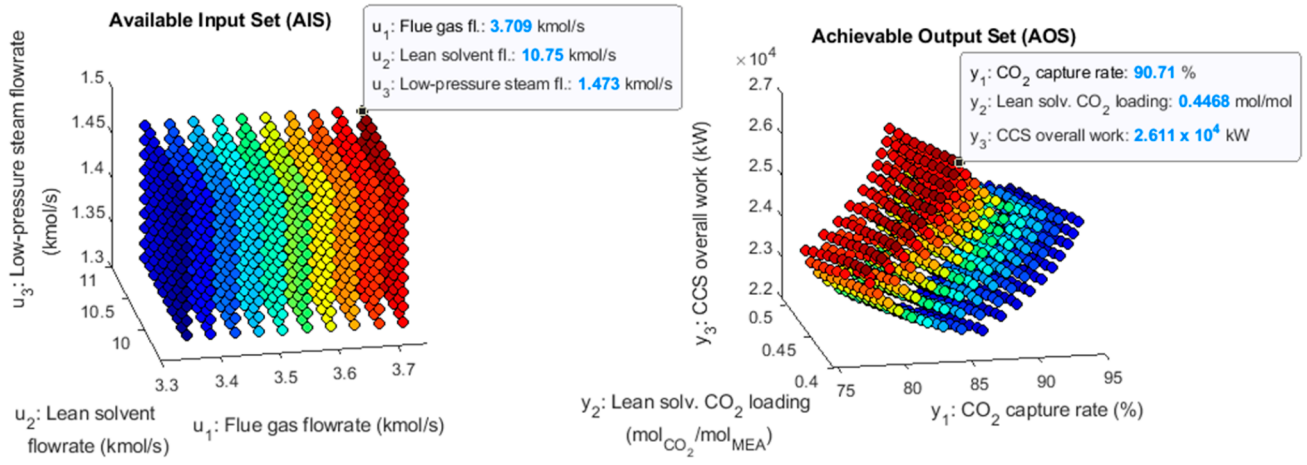

Figure 7. Input−output mapping of CCS unit.

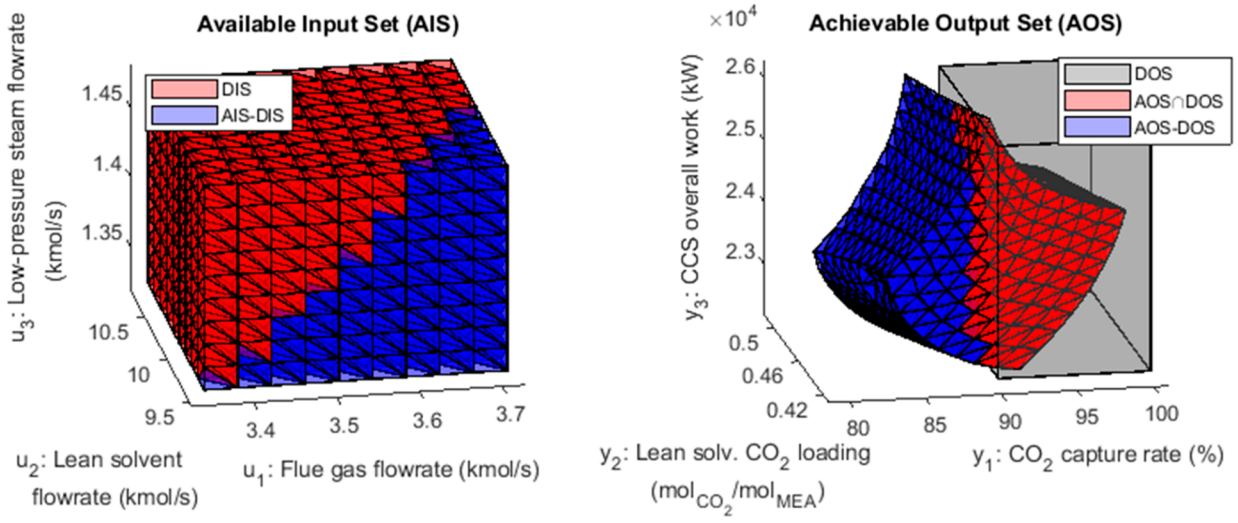

Figure 8. Steady-state achievability of 90% of CO_2 capture rate.

coal-fired power plant, and the other two are manipulated variables. Here, u_1 is not assigned to the EDS as it is assumed to be controlled by other portions of the plant. Moreover, this variable has a specific expected profile that has higher values in the periods of morning and night when solar energy generation is low and energy demand is high.[36]

With the Operability App, the reduced order model is uploaded, and the input variable ranges are discretized. The plant behavior is simulated for several combinations of inputs within the formed grid, generating the input−output mapping shown in Figure 7. In this figure, the color code indicates the correspondence between the mapped input and output points.

For each value u_1 of the flue gas flow rate, the ranges of lean solvent flow rate and low-pressure steam flow rate can be combined to form a 2-dimensional space of possibilities where these two manipulated variables can be set. In Figure 7, such spaces are represented in the AIS by "flat sheets" of color blue, light blue, green, yellow, and so on.

The corresponding outputs are also in sheet surfaces that are distributed in the AOS. For low values of the flue gas flow rate (dark blue points in Figure 7), the achievable space is a surface located in an AOS region of higher CO_2 capture rate and smaller values for the lean solvent CO_2 loading and CCS overall work. Conversely, high values of the flue gas flow rate (red points in Figure 7) generate an AOS surface in which the CO_2 capture rate is lower and the lean solvent CO_2 loading and CCS overall work are higher. This behavior indicates that the considered design is capable of achieving higher CO_2 capture rates with smaller operating costs as expected when lower amounts of flue gas have to be processed; while higher amounts of flue gas limit the achievable CO_2 capture rates and increase the operating cost of the unit associated with the lean solvent CO_2 loading and CCS overall work.

To quantify the limited achievability for the CO_2 capture rate, the worst-case scenario for the variable u_1 (corresponding to the flue gas flow rate of around 3.7 kmol/s) is analyzed. Figure 7 contains a highlighted point that corresponds to a possible maximum CO_2 capture rate for this scenario. Note that when the CCS unit receives a flue gas flow rate at its highest expected value, the MVs of the lean solvent flow rate and low-pressure steam flow rate can be set to their corresponding upper limits to achieve a maximum CO_2 capture of around 90.7%.

To further verify the limitation on CO_2 capture rates of the CCS design, a DOS is first set to a minimum value of CO_2 capture rate of 90% and then slightly increased to a rate of 92%. The input−output mapping is converted to the multimodel representation and, for each case, the achievability of the DOS is evaluated. The DIS is also calculated for each case, consisting of

DOI: 10.1021/acs.iecr.9b05181
Ind. Eng. Chem. Res. 2020, 59, 2457−2470

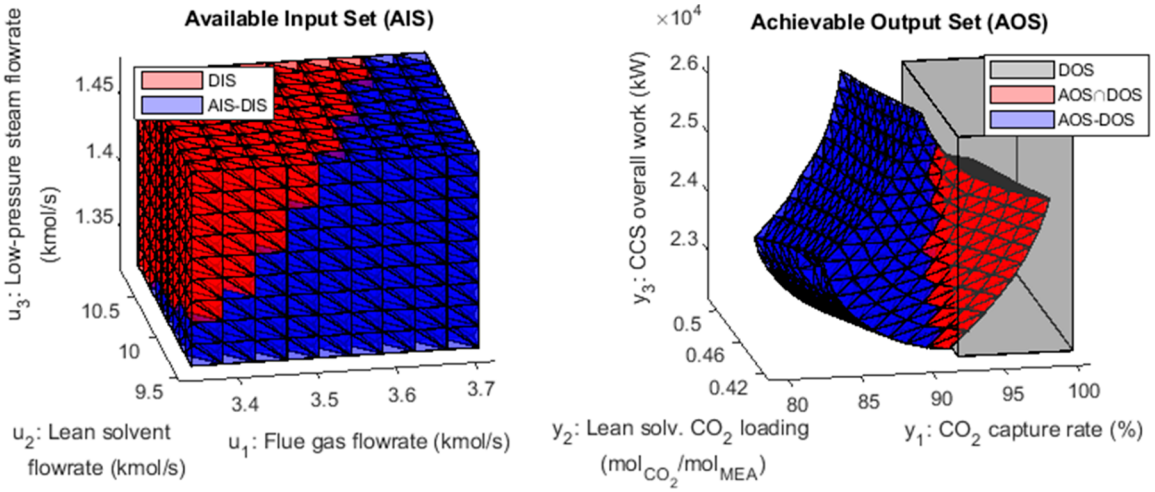

Figure 9. Steady-state achievability of 92% of CO_2 capture rate.

the input region that would be needed to achieve the analyzed DOS. For both DOS's, the Operability App is employed to perform the analysis and generate the plots.

Figure 8 shows the operability analysis for a CO_2 capture rate equal to or higher than 90%. In this figure, the red and blue regions refer to the portions that achieve and do not achieve the CO_2 capture goal, respectively. The higher the values of flue gas flow rate, the more restricted is the available region to achieve the desired CO_2 capture rate of 90%. Moreover, the needed values for the MVs of lean solvent flow rate and low-pressure steam flow rate are more limited and closer to their upper bounds as the flue gas flow rate increases.

Figure 9 depicts a similar study for the desired CO_2 capture rate of 92%. By inspecting the AIS regions, it is possible to see that for values of flue gas flow rate in the range around 3.62−3.7 kmol/s, there are no combinations of lean solvent flow rate and low-pressure steam flow rate that can take the system response to the DOS (all combinations are in blue, outside of the DIS). Therefore, for this flue gas configuration, the CCS design is not capable of achieving the CO_2 capture rate of 92%.

From the employed operability analysis, considering all flue gas flow rate scenarios, the current CCS design is able to achieve the standard CO_2 capture rate of 90% with the available ranges of lean solvent and low-pressure steam flow rates. However, this CCS design is not able to achieve CO_2 capture rates above 91% for all the flue gas flow rate scenarios. To enable higher CO_2 capture rates, process design changes would have to considered such as enlarging the available ranges of MVs or changing the CCS design, for instance, by increasing the number of separation trains. The operability method and Operability App can thus provide insights on how these modifications could be performed.

6. CONCLUSIONS AND FUTURE DEVELOPMENTS

In this Article, a review of current process operability algorithms was provided. The most recent algorithms were further developed and adapted to be compiled as part of an open-source operability platform. This platform grants access to operability approaches and algorithms, motivating the dissemination of these algorithms and improvements in the process operability field. The developed Operability App in MATLAB corresponds to the first effort to include contributions of other researchers that have worked in operability in the past or intend to do in the future.

The addressed applications showed versatility of the developed Operability App, which can reproduce previous literature results, easily switch from one setting to another and tackle new process models. The comparison of measures of OI indicated that specific cases may not be compatible to the original interpretation of the OI in terms of volume and hypervolume, being suitable for the alterative measure using DOS subregions. To deal with the challenge of infeasible DOS regions, the feasible DOS, DOS*, was found and later used for the determination of the design and nominal operation that achieve SM and PI targets while respecting process constraints. The CCS application associated with the coal-fired power plant cycling demonstrated how reduced-order or surrogate models can be employed for achievability analysis, generating meaningful results without necessarily employing OI calculations.

Although the multimodel and NLP-based approaches were generalized in terms of dimensionalities and process model nature, it is still not clear what would be the upper limit in the capability of the employed algorithms. There is also the possibility of including other process operability algorithms associated with process dynamics and interval-control. Tractability for higher dimensionalities and the consideration of systems that must be operated around singularities or discontinuous spaces are highlighted as potential critical limitations for the evaluation of existing operability algorithms.

Improvements regarding theory and software infrastructure consist of other future directions. The inclusion of the EDS can be done by considering the process stochastic behavior, allowing operability to be a tool for interfacing design and control under uncertainty. Both the multimodel and NLP-based approaches would benefit from other input−output system representations, especially for the representation of high-dimensional processes. Particular extensions are suitable to the MILP-based algorithms, such as the examination of other ways to increase space resolution and the adaptation to mixed-integer nonlinear programming (MINLP)-based formulations.

Prospective directions toward the incorporation of process operability concepts into other areas are also considered. Both dynamic and steady-state process operability concepts could be integrated with operator advisory systems, enabling the improvement of plant operation. There is also an opportunity

DOI: 10.1021/acs.iecr.9b05181
Ind. Eng. Chem. Res. 2020, 59, 2457−2470

to integrate process operability with real-time model-based control algorithms such as dynamic real-time optimization (DRTO).

AUTHOR INFORMATION

Corresponding Author

*E-mail: fernando.lima@mail.wvu.edu.

ORCID

Fernando V. Lima: 0000-0003-4306-1826

Notes

The authors declare no competing financial interest.

ACKNOWLEDGMENTS

The authors gratefully acknowledge the Donors of the American Chemical Society Petroleum Research Fund and the National Science Foundation CAREER Award 1653098 for partial support of this research. Acknowledgements are also made for the financial support from U.S.-China Clean Energy Research Center (CERC) program and U.S. Department of Energy under Cooperative Agreement DEPI0000017. The authors are also grateful to Rebecca H. H. Kim (WVU Ph.D. candidate) for help in providing reduced models and conditions for proper simulation of the CCS process model.

REFERENCES

(1) Tonkovich, A. Y.; Perry, S.; Wang, Y.; Qiu, D.; Laplante, T.; Rogers, W. A. MicroChannel Process Technology for Compact Methane Steam Reforming. *Chem. Eng. Sci.* **2004**, *59*, 4819.

(2) Baldea, M.; Edgar, T. F.; Stanley, B. L.; Kiss, A. A. Modular Manufacturing Processes: Status, Challenges, and Opportunities. *AIChE J.* **2017**, *63*, 4262.

(3) Vinson, D. R.; Georgakis, C. New Measure of Process Output Controllability. *J. Process Control* **2000**, *10*, 185.

(4) Vinson, D. R.; Georgakis, C. Inventory Control Structure Independence of the Process Operability Index. *Ind. Eng. Chem. Res.* **2002**, *41*, 3970.

(5) Subramanian, S.; Georgakis, C. Steady-State Operability Characteristics of Idealized Reactors. *Chem. Eng. Sci.* **2001**, *56*, 5111.

(6) Georgakis, C.; Uztürk, D.; Subramanian, S.; Vinson, D. R. On the Operability of Continuous Processes. *Control Eng. Pract.* **2003**, *11*, 859.

(7) Uztürk, D.; Georgakis, C. Inherent Dynamic Operability of Processes: General Definitions and Analysis of SISO Cases. *Ind. Eng. Chem. Res.* **2002**, *41*, 421.

(8) Lima, F. V.; Georgakis, C. Dynamic Operability for the Calculation of Transient Output Constraints for Non-Square Linear Model Predictive Controllers. *IFAC Proceedings Volumes* **2009**, *42* (11), 231−236.

(9) Lima, F. V.; Jia, Z.; Ierapetritou, M.; Georgakis, C. Similarities and Differences between the Concepts of Operability and Flexibility: The Steady-State Case. *AIChE J.* **2010**, *56*, 702.

(10) Gazzaneo, V.; Lima, F. V. Multilayer Operability Framework for Process Design, Intensification, and Modularization of Nonlinear Energy Systems. *Ind. Eng. Chem. Res.* **2019**, *58*, 6069.

(11) Davis, E.; Ierapetritou, M. A Kriging Method for the Solution of Nonlinear Programs with Black-Box Functions. *AIChE J.* **2007**, *53*, 2001.

(12) Boukouvala, F.; Muzzio, F. J.; Ierapetritou, M. G. Design Space of Pharmaceutical Processes Using Data-Driven-Based Methods. *J. Pharm. Innov.* **2010**, *5*, 119.

(13) Georgakis, C. Design of Dynamic Experiments: A Data-Driven Methodology for the Optimization of Time-Varying Processes. *Ind. Eng. Chem. Res.* **2013**, *52*, 12369.

(14) Kiparissides, A.; Georgakis, C.; Mantalaris, A.; Pistikopoulos, E. N. Design of in Silico Experiments as a Tool for Nonlinear Sensitivity Analysis of Knowledge-Driven Models. *Ind. Eng. Chem. Res.* **2014**, *53*, 7517.

(15) Goyal, V.; Ierapetritou, M. G. Determination of Operability Limits Using Simplicial Approximation. *AIChE J.* **2002**, *48*, 2902.

(16) Banerjee, I.; Ierapetritou, M. G. Design Optimization under Parameter Uncertainty for General Black-Box Models. *Ind. Eng. Chem. Res.* **2002**, *41*, 6687.

(17) Li, Z.; Ierapetritou, M. G. A New Methodology for the General Multiparametric Mixed-Integer Linear Programming (MILP) Problems. *Ind. Eng. Chem. Res.* **2007**, *46*, 5141.

(18) Pistikopoulos, E. N.; Diangelakis, N. A. Towards the Integration of Process Design, Control and Scheduling: Are We Getting Closer? *Comput. Chem. Eng.* **2016**, *91*, 85.

(19) Georgakis, C.; Li, L. On the Calculation of Operability Sets of Nonlinear High-Dimensional Processes. *Ind. Eng. Chem. Res.* **2010**, *49*, 8035.

(20) Carrasco, J. C.; Lima, F. V. Bilevel and Parallel Programing-Based Operability Approaches for Process Intensification and Modularity. *AIChE J.* **2018**, *64*, 3042.

(21) Carrasco, J. C.; Lima, F. V. Operability-Based Approach for Process Design, Intensification, and Control: Application to High-Dimensional and Nonlinear Membrane Reactors. In *Proceedings of the FOCAPO/CPC* 2017.

(22) Carrasco, J. C.; Lima, F. V. An Optimization-Based Operability Framework for Process Design and Intensification of Modular Natural Gas Utilization Systems. *Comput. Chem. Eng.* **2017**, *105*, 246.

(23) Carrasco, J. C.; Lima, F. V. Novel Operability-Based Approach for Process Design and Intensification: Application to a Membrane Reactor for Direct Methane Aromatization. *AIChE J.* **2017**, *63*, 975.

(24) Gazzaneo, V.; Carrasco, J. C.; Lima, F. V. An MILP-Based Operability Approach for Process Intensification and Design of Modular Energy Systems. *Comput.-Aided Chem. Eng.* **2018**, 2371.

(25) Lima, F. V.; Georgakis, C. Input-Output Operability of Control Systems: The Steady-State Case. *J. Process Control* **2010**, *20*, 769.

(26) Subramanian, S.; Georgakis, C. Methodology for the Steady-State Operability Analysis of Plantwide Systems. *Ind. Eng. Chem. Res.* **2005**, *44*, 7770.

(27) Subramanian, S.; Uztürk, D.; Georgakis, C. An Optimization-Based Approach for the Operability Analysis of Continuously Stirred Tank Reactors. *Ind. Eng. Chem. Res.* **2001**, *40*, 4238.

(28) Lima, F. V.; Georgakis, C. Design of Output Constraints for Model-Based Non-Square Controllers Using Interval Operability. *J. Process Control* **2008**, *18*, 610.

(29) Herceg, M.; Kvasnica, M.; Jones, C.; Morari, M. Multi-Parametric Toolbox 3.0. *Proceedings of the European Control Conference*; ECC, 2013; DOI DOI: 10.23919/ECC.2013.6669862.

(30) Carrasco, J. C.; Lima, F. V. Nonlinear Operability of a Membrane Reactor for Direct Methane Aromatization. *IFAC-PapersOnLine* **2015**, *48*, 728.

(31) He, X.; Lima, F. V. Development and Implementation of Advanced Control Strategies for Power Plant Cycling with Carbon Capture. *Comput. Chem. Eng.* **2019**, *121*, 497.

(32) Li, L.; Borry, R. W.; Iglesia, E. Design and Optimization of Catalysts and Membrane Reactors for the Non-Oxidative Conversion of Methane. *Chem. Eng. Sci.* **2002**, *57*, 4595.

(33) Li, J.; Yoon, H.; Wachsman, E. D. Hydrogen Permeation through Thin Supported SrCe0.7Zr0.2Eu0.1O3-δ Membranes; Dependence of Flux on Defect Equilibria and Operating Conditions. *J. Membr. Sci.* **2011**, *381*, 126.

(34) Rawlings, J. B.; Ekerdt, J. G. *Chemical Reactor Analysis and Design Fundamentals*; Nob Hill Publishing: Madison, WI, USA, 2002.

(35) Carrasco, J. C. Operability-Based Design of Energy Systems: Application to Natural Gas Utilization Processes, *Ph.D. Thesis*, West Virginia University, 2017.

(36) Kim, R.; Lima, F. V. A Tchebycheff-Based Multi-Objective Combined with a PSO-SQP Dynamic Real-Time Optimization Framework for Cycling Energy Systems. Submitted for publication.

DOI: 10.1021/acs.iecr.9b05181
Ind. Eng. Chem. Res. 2020, 59, 2457−2470